Journal of Experimental Botany, Vol. 74, No. 3 pp. 976–990, 2023
https://doi.org/10.1093/jxb/erac442 Advance Access Publication 8 November 2022

RESEARCH PAPER

Glutathione and neodiosmin feedback sustain plant immunity

Chongchong Lu[1], Yanke Jiang[1], Yingzhe Yue[1], Yurong Sui[1], Mingxia Hao[1], Xiaojing Kang[1], Qingbin Wang[1,2], Dayin Chen[2], Baoyou Liu[1,3], Ziyi Yin[1], Lulu Wang[1], Yang Li[1], Hansong Dong[1], Xugang Li[1], Xiufang Xin[4], Yinggao Liu[1] and Xinhua Ding[1,*]

[1] State Key Laboratory of Crop Biology, Shandong Provincial Key Laboratory for Biology of Vegetable Diseases and Insect Pests, College of Plant Protection, Shandong Agricultural University, Taian, Shandong 271018, China
[2] Shandong Pengbo Biotechnology Co., Ltd, Taian, Shandong 271018, China
[3] Yantai Academy of Agricultural Sciences, Yantai, Shandong 265500, China
[4] National Key Laboratory of Plant Molecular Genetics, Chinese Academy of Sciences Center for Excellence in Molecular Plant Sciences, Institute of Plant Physiology and Ecology, Chinese Academy of Sciences, Shanghai 200032, China

* Correspondence: xhding@sdau.edu.cn

Received 6 July 2022; Editorial decision 24 October 2022; Accepted 5 November 2022

Editor: Toshihiro Obata, University of Nebraska-Lincoln, USA

Abstract

Plants have evolved a two-layer immune system comprising pattern-triggered immunity (PTI) and effector-triggered immunity (ETI) that is activated in response to pathogen invasion. Microbial patterns and pathogen effectors can be recognized by surface-localized pattern-recognition receptors (PRRs) and intracellularly localized nucleotide-binding leucine-rich repeat receptors (NLRs) to trigger PTI and ETI responses, respectively. At present, the metabolites activated by PTI and ETI and their roles and signalling pathways in plant immunity are not well understood. In this study, metabolomic analysis showed that ETI and PTI induced various flavonoids and amino acids and their derivatives in plants. Interestingly, both glutathione and neodiosmin content were specifically up-regulated by ETI and PTI, respectively, which significantly enhanced plant immunity. Further studies showed that glutathione and neodiosmin failed to induce a plant immune response in which PRRs/co-receptors were mutated. In addition, glutathione-reduced mutant *gsh1* analysis showed that *GSH1* is also required for PTI and ETI. Finally, we propose a model in which glutathione and neodiosmin are considered signature metabolites induced in the process of ETI and PTI activation in plants and further continuous enhancement of plant immunity in which PRRs/co-receptors are needed. This model is beneficial for an in-depth understanding of the closed-loop mode of the positive feedback regulation of PTI and ETI signals at the metabolic level.

Keywords: Effector-triggered immunity, glutathione, metabolites, neodiosmin, pattern-triggered immunity, plant immunity.

Introduction

Plants generally counteract pathogen infection by inducing the activity of their innate immune system, which involves pattern-triggered immunity (PTI) and effector-triggered immunity (ETI) (Jones and Dangl, 2006; Monaghan and Zipfel, 2012). PTI and ETI are a plant's two-layer immune system and rely on the recognition of membrane-localized pattern-recognition receptors/co-receptors (PRRs/co-receptors) to detect conserved molecules, termed microbe-associated (or

pathogen-associated) molecular patterns (MAMPs/PAMPs), and nucleotide-binding, leucine-rich repeat receptors (NLRs) to recognize characteristic type III effectors (T3Es), further inducing the plant immune response (Segonzac and Zipfel, 2011; Couto and Zipfel, 2016; Jones *et al.*, 2016). Both PTI and ETI induce reactive oxygen species (ROS) and Ca^{2+} bursts, callose deposition, phosphorylation cascades involving mitogen-activated kinases (MPKs), biosynthesis of phytohormones, and transcriptional activation of downstream defence-related genes (Jones and Dangl, 2006; Monaghan and Zipfel, 2012;Yuan *et al.*, 2021), which suggests that ETI and PTI share many common signalling pathways involved in the regulation of plant immunity. During the coevolution of pathogens and plants, pathogens evolved a type III secretion system (T3SS) that secretes virulence molecules, including T3Es, exopolysaccharides, and toxins (Segonzac and Zipfel, 2011), which are injected into plant cells to subvert the plant immune response.

ETI usually induces a stronger response than PTI via recognition of individual T3Es by matching resistance proteins (Dodds and Rathjen, 2010), leading to programmed cell death, a phenomenon termed the hypersensitive response (HR) (Jones and Dangl, 2006). ETI and PTI share some downstream signalling response crosstalk with salicylic acid (SA) signalling pathways (Tsuda and Katagiri, 2010). For instance, the amino acid peptide FLAGELLIN 22 (Flg22) was identified as a PAMP that activates PTI in plants and triggers SA production. On the other hand, an HR was associated with the biosynthesis of SA (Mur *et al.*, 2000), which enhances plant resistance against biotrophic and hemi-biotrophic pathogens (Segonzac and Zipfel, 2011; De Vleesschauwer *et al.*, 2016). In addition, the SA receptors NPR3 and NPR4 promote the degradation of JASMONATE ZIM DOMAIN proteins (JAZs) to enhance the ETI response (Liu *et al.*, 2016). Most notably, recently published studies have shown that PRRs/co-receptors are indispensable components involved in the activation of ETI and have proven that PTI plays an important positive role in the process of enhancing ETI (Ngou *et al.*, 2021;Yuan *et al.*, 2021).

Genome-wide transcriptome profiling is an efficient approach for determining biological processes at the level of gene expression in cells under different treatments (Ansorge, 2009; Wang *et al.*, 2009; Haas and Zody, 2010; Pombo *et al.*, 2014). A recent report showed that transcriptomic analysis revealed a series of genes induced specifically by ETI and identified *Epk1*, which encodes a protein kinase that plays a unique role in the bacterial effector-triggered response (Pombo *et al.*, 2014). Moreover, transcriptome profiling of a *Pseudomonas syringae* strain has revealed specific bacterial processes and genes that are differentially expressed during ETI and PTI (Nobori *et al.*, 2018). Notably, pathogen invasion and activation of the immune response not only induces large amounts of gene transcriptional reprogramming but also leads to a large number of differentially accumulated metabolites. Some metabolites have been extensively studied for their role in immunity against bacterial pathogens, such as phytosterols (Griebel and Zeier, 2010), coumarins (Chaouch *et al.*, 2012), indols (Stahl *et al.*, 2016), and amino acids (Navarova *et al.*, 2012). Recently, a multiomics strategy was used to systematically analyse the PTI response mechanism in the process of rice disease resistance (Tang *et al.*, 2021). However, the role of ETI- and PTI-activated metabolites in the regulation of plant immunity is still unclear. Are there metabolites produced in ETI that are perceived by PRRs/co-receptors to amplify ETI responses (Chang *et al.*, 2021)? Therefore, metabolomic analysis has been used to identify the differentially accumulated metabolites induced by ETI and PTI and further demonstrate the role of the key metabolites involved in the regulation of the plant immune response, which will help to better understand the roles of metabolites involved in the feedback regulation of plant ETI and PTI at the metabolic level.

Glutathione is composed of three amino acids (glutamate, cysteine, and glycine), and plays a wide role in eukaryotes. Glutathione biosynthesis requires the following two adenosine triphosphate dependent enzymes: γ-glutamylcysteine synthetase glutathione (GSH1) and glutathione synthetase glutathione (GSH2) (Zhu *et al.*, 2021). Glutathione plays an important role in plant growth and development, tolerance to abiotic stresses, and defence reactions against biotic stress (Kocsy *et al.*, 2000; Clay *et al.*, 2009; Noctor *et al.*, 2012; Zechmann, 2014; Cheng *et al.*, 2015; Mukaihara *et al.*, 2016; Kunstler *et al.*, 2019). Neodiosmin (other names: diosmetin-7-neohesperidoside, NEO) is a flavonoid with antioxidant properties and was first isolated from *Citrus aurantium* leaves (Raithore *et al.*, 2020; Huang *et al.*, 2021). However, the role of glutathione and NEO in the regulation of plant ETI and PTI is not clear.

Interactions between *Pseudomonas syringae* pv. *tomato* (*Pst*) and its host plants have been used extensively to study host immune responses to bacterial infection (Pedley and Martin, 2003; Oh and Martin, 2011). The *Pst* DC3000 strain delivers T3Es into tomato cells, and two of these effectors, AvrPto and AvrPtoB, impede pattern recognition receptor function, thereby undermining the PTI response and promoting bacterial infection (Cunnac *et al.*, 2011; Oh and Martin, 2011; Rosli *et al.*, 2013). However, *Pst* DC3000 (*avrRpt2*) and *Pst* DC3000 (*avrRps4*) secrete AvrRpt2 and AvrRps4, which are recognized by RPS2 and RPS4 and cause a signalling cascade to induce the ETI response (Gassmann *et al.*, 1999; Axtell and Staskawicz, 2003; Mackey *et al.*, 2003). Another *Pst* strain, D36E, has 36 fewer effector factor-encoding genes than *Pst* DC3000 and can activate only plant PTI (Wei *et al.*, 2015). By using the abovementioned bacterial strains, we used metabolomic analysis to determine the differences in metabolite accumulation in plants inoculated with *Pst* DC3000, D36E, *Pst* DC3000 (*avrRpt2*) and *Pst* DC3000 (*avrRps4*). By performing metabolomic analysis, we found that D36E, *Pst* DC3000 (*avrRpt2*) and *Pst* DC3000 (*avrRps4*) induced the accumulation of flavonoids and amino acids and their derivatives in plant leaves. Venn diagrams combined with the results from a heatmap analysis showed that ETI and PTI typically induced the accumulation

of glutathione and NEO, both of which activate ROS bursts and MPK phosphorylation and up-regulate the expression of PTI-ETI-induced genes in Arabidopsis ecotype Columbia (Col-0), but were compromised in PRR/co-receptor mutants. Furthermore, the glutathione-reduced mutant *gsh1* was also required for the plant immunity response. These observations help reveal a novel mechanism in which ETI and PTI induce similar or unique accumulations of plant immunity-associated metabolites to sustain the plant immune response.

Materials and methods

Plant materials and growth conditions

Arabidopsis (*Arabidopsis thaliana*) Col-0 seeds were sterilized in 75% ethanol for 1 min, washed three times with double distilled water, immersed in a 1.5% NaClO solution for 15 min and washed six to seven times with double distilled water. After surface sterilization, the seeds were sown on square Petri dishes that contained 20 ml of 1/2-strength Murashige and Skoog (MS) media. The seeds were vernalized for 2 d at 4 °C before germination. After 7 d of germination, the seedlings were transferred to vermiculite plus 1/4-strength MS culture media without sucrose or agar. The seedlings were then grown under the following conditions: 21 °C, 60–70% humidity, and a 12 h light photoperiod. *fls2 efr cerk1* (*fec*), *bak1 bkk1 cerk1* (*bbc*), and *rps2* mutants were generated by the staff of the Cyril Zipfel laboratory (Schwessinger *et al.*, 2011), the *rbohd* mutant was generated by the staff of the Xiufang Xin laboratory (Yuan *et al.*, 2021), and *gsh1* (*cad2-1*) was generated by the Barbara Rolls laboratory (Cobbett *et al.*, 1998).

Bacterial growth assays

Four-week-old Arabidopsis plants were infiltrated with *Pst* DC3000 at an OD_{600} of 0.001. Two hours later, they were sprayed with water, oxidized glutathione (GSSG), GSH or NEO, after which diseased leaves were harvested at 3 d post-incubation (dpi) and surface sterilized in a 75% ethanol solution for 1 min. Afterwards, the diseased leaves were washed three times with double distilled water. A surface-sterilized mortar was used to crush the diseased leaves into a homogenized sample in double distilled water. The homogenate was then continuously diluted (1:10) seven to eight times, and a 10 µl aliquot was plated onto polypeptone sucrose agar media for counting individual colonies after they were allowed to grow for 1–2 d at 28 °C. For the bacterial growth inhibition experiment, the *Pst* DC3000 (OD=1) suspension was diluted (10%) four to five times and then plated onto PSA media supplemented with 0, 1, 10, 100, and 200 ng/mL GSSG, GSH, or NEO. The growth of bacterial colonies was counted after 24 h. The experiment was performed in three biological replicates.

ROS staining

H_2O_2 and O_2^- were detected via 3,3-diaminobenzidine (DAB) and nitro blue tetrazolium (NBT) staining, respectively (Lu *et al.*, 2019). For NBT staining, 10-day-old seedlings were harvested from treated plants at 2 h post-treatment (hpt). The seedlings were then immediately put into a sodium azide solution (1%) and subsequently into a vacuum chamber for 30 min. Afterwards, the leaves were transferred to a 0.5 mg/mL NBT staining solution and placed in a vacuum chamber again for 30 min. For DAB staining, the harvested seedlings were transferred to a 1 mg/mL DAB staining solution and placed in a vacuum chamber for 30 min. Afterwards, the seedlings were transferred to a 28 °C incubator under light for 8 h. After the reaction was complete, excess dye solution was discarded, and the seedlings were washed with boiling ethanol. Finally, the seedlings were imaged by a stereomicroscope (Nikon, Japan). ROS levels were detected at 2 hpi with different treatments. Plant leaves were infiltrated with 1 µM fluorescent dye 2',7'-Dichlorodihydrofluorescein diacetate (H_2DCFDA) solution, and the fluorescence signal was detected 10 min later with a Zeiss LSM880 laser scanning microscope (488 nm excitation wavelength and 501–550 nm emission wavelengths). Chloroplast autofluorescence (red) was excited at 543 nm and recorded at 640–735 nm. The above experiments were performed in three biological replicates.

Callose accumulation detection

Solution A contained deionized water (52%), lactic acid (20%), phenol (20%), and 8% glycerol (v/v). Following 50 µM GSH, GSSG, and NEO treatments for 24 h, the treated leaves were harvested and immersed in solution B (solution A: ethanol=1:2) under vacuum for 30 min. The above mixture was then incubated at 60 °C and mixed every 5 min for 30 min. The samples were washed for three times with deionized water. Clean leaves were placed in 0.01% aniline blue staining solution (150 mM K_2HPO_4 with pH=9.5). Callose deposition was imaged using a Zeiss LSM880 laser scanning microscope. The excitation wavelength was 405 nm, and the emission wavelength was 415–485 nm. Fluorescence intensity was quantified using ImageJ software.

Quantitative analysis of glutathione and NEO by high-performance liquid chromatography

Leaf samples (0.5–1 g) were frozen with liquid nitrogen, rapidly ground to a homogeneous powder, and transformed into a 1.5 ml centrifuge tube with 1 ml of 70% (v/v) methanol. The sample homogenate was inverted and mixed for 2–16 h at 4 °C and centrifuged at 14000 ×g for 20 min at 4 °C. Then, the supernatant was transferred into a new sterilized 2 ml centrifuge tube. The precipitate from the previous step was recovered, and the steps above were repeated. The two supernatants were merged into the same centrifuge tube. For GSSG and GSH detection, the chromatographic column used for high-performance liquid chromatography (HPLC) on a Shimadzu LC-20AD liquid chromatograph (ZORBAXSB-C18 4.6 × 50 mm, Agilent Technologies, USA), the operating temperature was 24 °C, the mobile phase contained formic acid (0.1%), water (98.9%), and methanol (1%), the flow rate was 1 ml/min, the detection wavelength was 200 nm, and the retention times of GSH and GSSG were 7.5 min and 13 min, respectively. For NEO detection, the operating temperature was 24 °C, and the mobile phases contained water (66%, v/v), acetonitrile (2%, v/v), glacial acetic acid (6%, v/v), and methanol (28%, v/v). The flow rate was 1 ml/min, the detection wavelength was 275 nm, and the retention time of NEO was 5 min.

Preparation and extraction of plant tissues for widely targeted metabolic analysis

To compare the metabolic differences that occur between PTI and ETI, Arabidopsis plants were grown for 28 d and injected with a suspension of *Pst* DC3000, *Pst* DC3000 (*avrRpt2*), *Pst* DC3000 (*avrRps4*), or D36E (OD=0.001, *Pst* DC3000). The experiment was repeated for three biological replicates, and leaves were harvested in each experiment at 2 h and 24 h. The leaves of seedlings before injection with *Pst* DC3000 (at 0 h) were used as a control (CK). The extraction method of Arabidopsis leaf metabolites was described in a previous article (Chen *et al.*, 2013). The samples were frozen in liquid N_2 and crushed to powder by a mixer mill (MM 400, Retsch) equipped with zirconia beads for 90 s at 30 Hz. Afterwards, 100 mg of powder was extracted overnight with 600 µl of 70% aqueous methanol at 4 °C. After centrifugation at 10 000 ×g for 10 min, the crude extracts were absorbed and filtered before ultra-performance

liquid chromatography (UPLC) and tandem mass spectrometry (MS/MS) analysis.

Widely targeted metabolic analysis

The sample extracts were sent to Metware Biotechnology Co., Ltd. (Wuhan, China), for further UPLC-MS/MS analysis, and the UPLC and MS/MS conditions were the same as those used in a previous report (Li *et al.*, 2018). Metabolites were identified using the Metware database and public databases in accordance with standard metabolic operating procedures.

MPK phosphorylation assays

Leaf discs (diameter=0.5 cm) from 4-week-old Arabidopsis plants were used for MPK phosphorylation assays (Liu *et al.*, 2015). First, the leaf discs were punched using a semi-automated puncher and then placed into 12-well plates with each well containing 2 ml of deionized water. Afterwards, they were incubated overnight and then transferred to new 12-well plates containing 2 ml of deionized water supplemented with H_2O, GSSG, GSH, and NEO. Samples were collected at the indicated times, and subsequently ground into a powder in liquid nitrogen. Total plant protein was extracted using a Plant Protein Extraction kit (CWBIO, China) according to the manufacturer's instructions. Coomassie brilliant blue (CBB) was used to calibrate the protein loading of each sample such that equal amounts were obtained. Equivalent amounts of protein were loaded onto a 15% SDS-PAGE gel for western blotting. MPK phosphorylation was detected using an anti-phospho-p44/42 antibody (Cell Signaling Technology, USA; 1/1000); goat anti-rabbit IgG horseradish peroxidase (Sigma, Japan; 1/10 000) was used as a secondary antibody. Following electrophoresis, the protein-containing gel was imaged with a Tanon-5200 imaging system.

RNA extraction and quantitative real-time PCR (qPCR)-based measurement of gene expression

To analyse gene expression levels, 4-week-old plants were sprayed with water, GSSG, GSH, or NEO, and then samples were collected at the indicated time points. Six leaves from different plants were collected three times (as three biological replicates). The leaf samples were subsequently ground into a powder in liquid nitrogen. Total RNA was extracted by using Monzol™ Reagent (MONAD, China) according to the manufacturer's instructions. Total RNA (1–2 μg) was reverse transcribed into cDNA using a MonScript™ RTIII Super Mix with dsDNase (MONAD). qPCR was then carried out in conjunction with UltraSYBR Mixture (CWBIO). The relative expression of genes was normalized at $2^{-\Delta Ct}$, $\Delta CT = CT_{target\ gene} - CT_{reference\ gene}$. The reference genes (*ACTIN* and *UBQ1*) were used for RT-qPCR assays. A QuantStudio 6 Flex Real-Time PCR System was used for qPCR, and three technical repeats were included for every sample.

Statistical analysis

The peak area was used to quantify metabolite abundance, and the data obtained from metabolite profiling were standardized for principal component analysis (PCA). Hierarchical cluster analysis of the different metabolites was performed, the results of which were visualized via heatmaps. The metabolite data were first $\log_2$ transformed, and differentially accumulated metabolites were identified by partial least squares-discriminate analysis. Metabolites whose accumulation significantly changed were determined based on a variable importance in projection (VIP) value ≥1 followed by both one-way ANOVA ($P \leq 0.05$) and a $\log_2$ (fold change) ≥1.

Results

Metabolomic analysis showed that flavonoids, lipids, phenols, alkaloids, and amino acids and their derivatives differentially accumulated during PTI and ETI

Four-week-old Arabidopsis (Col-0) plants were inoculated with four *Pst* strains: *Pst* DC3000, *Pst* DC3000 (*avrRpt2*), *Pst* DC3000 (*avrRps4*), and D36E. UPLC-MS/MS was performed to evaluate the dynamic metabolite changes in Arabidopsis leaves after inoculation with *Pst* DC3000, *Pst* DC3000 (*avrRpt2*), *Pst* DC3000 (*avrRps4*), or D36E at 2 hpt and 24 hpt. Pearson's correlation coefficients were used to assess the correlations between data sets (Supplementary Fig. S1A). Through PCA, we further determined the total differentially accumulated metabolites and the variation among each group of samples (Supplementary Fig. S1B). The 27 samples were separated, and each of them consisted of a cluster, suggesting that the materials had sufficient reproducibility, conforming to the requirements for subsequent quantitative analysis. The cluster heatmap represented a total of 442 metabolites that accumulated differently in the leaves of plants inoculated with *Pst* DC3000, *Pst* DC3000 (*avrRpt2*), *Pst* DC3000 (*avrRps4*), and D36E compared with the leaves of Arabidopsis control plants at 2 hpt and 24 hpt (Fig. 1A). The 442 identified metabolites could be categorized into 12 groups, and among these metabolites, flavonoids (17%), lipids (14%), phenolic acids (13%), amino acids and their derivatives (12%), and alkaloids (8%) accounted for the majority (Fig. 1B).

Amino acid metabolism is essential for most organisms. By performing metabolomic analysis, we found that all four *Pst* strains could induce significant changes in amino acid content. To further show the changes in amino acid content intuitively, a heatmap based on the Kyoto Encyclopedia of Genes and Genomes (KEGG) pathway of amino acid metabolism was constructed. The four *Pst* strains significantly induced the accumulation of neutral amino acids such as leucine, isoleucine, cysteine, tryptophan, and tyrosine, and alkaline amino acids (arginine) at 2 hpt and 24 hpt (Supplementary Fig. S2). As described previously (Navarova *et al.*, 2012), these results indicate that pathogen invasion can also directly modulate amino acid metabolism in plants.

Glutathione and NEO were specifically induced by ETI or PTI

To further demonstrate the regulatory effect of ETI and PTI on plant metabolism, a heatmap cluster analysis was conducted to further assess the patterns of differentially accumulated metabolites between ETI and PTI. A total of 77 differentially accumulated metabolites were detected in the *Pst* DC3000 (*avrRpt2*)/*Pst* DC3000, *Pst* DC3000 (*avrRps4*)/*Pst* DC3000, and D36E/*Pst* DC3000 groups, which mainly contained

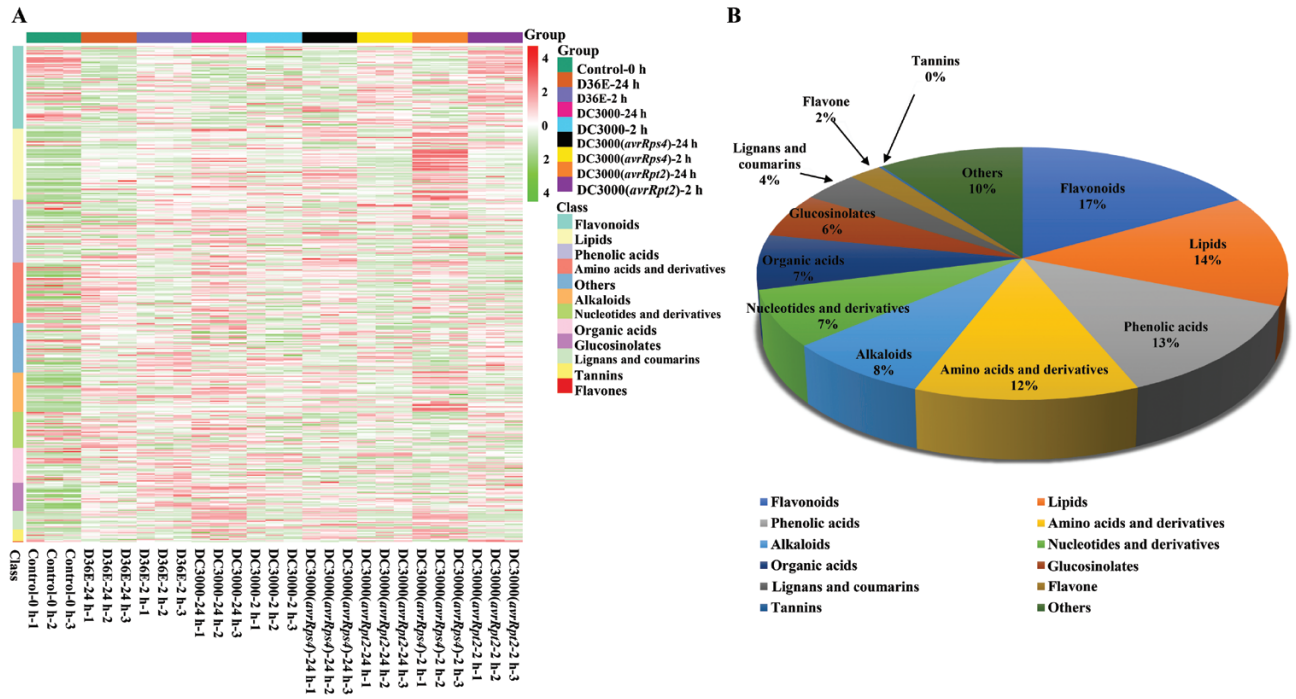

Fig. 1. Profiling of metabolomic data. (A) Heatmap showing 442 metabolites that differentially accumulated after treatment with different *Pst* strains. (B) Pie chart showing the percentage of each category.

flavonoids (number=14), phenolic acids (number=8), nucleotides and their derivatives (number=3), and amino acids and their derivatives (number=4) at 2 hpt (Fig. 2A-C), and flavonoids (number=14), lipids (12), amino acids and their derivatives (number=5), and phenolic acids (number=4) at 24 hpt (Fig. 2D-F), respectively. Among them, *Pst* DC3000 (*avrRpt2*), *Pst* DC3000 (*avrRps4*), and D36E significantly improved flavonoid (NEO, hispidulin, ladanein, eupatorin, isorhamnetin 3-*O*-neohesperidoside) accumulation at both 2 hpt and 24 hpt (Fig. 2), and reduced flavonoid (cyanin chloride) accumulation at 24 hpt (Fig. 2D-F). In addition, *Pst* DC3000 (*avrRpt2*), *Pst* DC3000 (*avrRps4*), and D36E also significantly induced amino acids and their derivatives (glutathione reduced form), nucleotides and their derivatives (2-deoxyribose 5-phosphate, uridine 5'-diphospho-D-glucose), and phenolic acids (3-hydroxy-4-isopropylbenzylalcohol 3-glucoside) at both 2 hpt and 24 hpt, and reduced neoglucobrassicin accumulation at 24 hpt (Fig. 2). In particular, *Pst* DC3000 (*avrRps4*) markedly induced lipid [LysoPE 18:1, MAG(18:3) isomer5, MAG(18:2)isomer1, LysoPE 18:1(2n isomer), LysoPC 16:2(2n isomer), LysoPC 18:3(2n isomer), LysoPE 18:2(2n isomer), MAG(18:3)isomer4, MAG(18:3)isomer1, 13-HOTrE(r), and PC(18:2)isomer] accumulation at 24 hpt (Fig. 2D). D36E significantly reduced alkaloids (indole-5-carboxylic acid, tryptophol, indole-3-carboxylic acid, and isoquinoline) and lignans and coumarins (pinoresinol, scopoline, 4-hydroxycoumarin, and syringaresinol) at 24 hpt (Fig. 2F). Together, these data indicated that the abovementioned differentially accumulated metabolites may play a role in ETI and PTI.

To further analyse the differentially accumulated metabolites whose accumulation was induced in response to the four *Pst* strains, a Venn diagram was constructed to help show differences and commonalities between the different groups. As shown in Fig. 3A, the Venn diagram shows the numbers of differentially accumulated metabolites in the different groups, and the heatmap (Fig. 3B) shows the typical changes in differentially accumulated metabolites in the *Pst* DC3000 (*avrRpt2*)/CK, *Pst* DC3000 (*avrRps4*)/CK, and D36E/CK combinations at 2 hpt and 24 hpt. Furthermore, we analysed differentially accumulated metabolites co- or specifically induced by ETI and PTI. We observed that both ETI and PTI could significantly induce pipecolic acid, glutathione reduced form (GSH), and 6-hydroxykaempferol-3,6-O-diglucoside accumulation (Fig. 3B). In addition, PTI specifically induced amino acids (N6-acetyl-L-lysine, oxidized glutathione), a glucosinolate (2-hydroxy-2-methylbutyl thioglucoside), an alkaloid (cocamidopropyl betaine), and organic acids (succinic acid and methylmalonic acid). ETI induced phenolic acids (3-hydroxy-4-isopropylbenzyl alcohol 3-glucoside and trans-4-hydroxycinnamic acid methyl ester), flavones (butin, 2,6-dimethyl-7-octene-2,3,6-triol, and NEO), an organic acid (arachidonic acid), and especially lipids [lysoPE 14:0, lauric acid, 9-KODE, lysoPE 16:0(2n isomer), eicosadienoic acid, and PC (18:2) isomer] (Fig. 3B). In addition, we also observed that *Pst* DC3000 (*avrRpt2*), *Pst* DC3000 (*avrRps4*), and D36E

Fig. 2. Differentially accumulated metabolite cluster analysis showing that both ETI and PTI significantly induced the accumulation of flavonoids, and amino acids and their derivatives. (A, D) Heatmaps representing the results of the cluster analysis of *Pst* DC3000 vs. *Pst* DC3000 (*avrRpt2*) at 2 hpt and 24 hpt, respectively. (B, E) Heatmaps representing the results of the cluster analysis of *Pst* DC3000 vs. *Pst* DC3000 (*avrRps4*) at 2 hpt and 24 hpt, respectively. (C, F) Heatmaps representing the results of the cluster analysis of *Pst* DC3000 vs. D36E at 2 hpt and 24 hpt, respectively. Pmp001274, 2-hydroxy-5,8,11,14,17-icosapentaenoyloxypropyl-2-(trimethylammonium)ethyl phosphate; Cmln001822, 6-(3,4-dihydroxyphenylacrylic acid)-β-D-1-thioglucoside of 4-(methylthio)-3-butenyl. The key metabolites mentioned in this article are shown in bold blue.

typically induced accumulations of GSH and NEO at both 2 hpt and 24 hpt compared with those in the *Pst* DC3000/CK combination (Fig. 3C), which suggests that both GSH and NEO may play a role in the response to ETI and PTI. To further compare the similarities and differences the functions of ETI- and PTI-induced metabolites in regulating plant immunity, GSSG (PTI-induced), NEO (ETI-induced), and GSH (PTI- and ETI-induced) were selected for the following experiment.

Glutathione and NEO induced plant immunity

To further prove that GSSG, GSH, and NEO were induced by ETI or PTI, we quantitatively detected their contents by HPLC. We observed that both *Pst* DC3000 (*avrRpt2*) and D36E significantly induced GSH accumulation (Fig. 4A), D36E specifically induced GSSG accumulation (Fig. 4B), and *Pst* DC3000 (*avrRpt2*) could specifically induce NEO accumulation (Fig. 4C), which was similar to the abovementioned results (Fig. 3B-C). To further reveal whether GSSG, GSH, and NEO enhance plant disease resistance, we inoculated Col-0 leaves with *Pst* DC3000 after exogenous applications of 0, 1, 10, and 50 μM GSSG, GSH, and NEO. The results showed that the population of surviving bacteria significantly decreased in number after GSSG, GSH, and NEO treatment (Fig. 4D-F), which demonstrated that GSSG, GSH, and NEO protect plants against bacterial infection.

To determine whether NEO, GSH, and GSSG can inhibit *Pst* DC3000 growth or induce plant immunity to defend against *Pst* DC3000 invasion, we first cultured *Pst* DC3000 in solid media that included 0, 1, 10, and 50 μM NEO, GSH, and GSSG. Surprisingly, the growth of *Pst* DC3000 did not decrease (Supplementary Fig. S3), suggesting that NEO, GSH, and GSSG (up to 50 μM) have no bacteriostatic activity and that the induction of plant resistance was probably plant dependent. To further investigate the role of NEO, GSH, and GSSG in triggering plant immunity, ROS production, MPK phosphorylation, callose accumulation, and the expression of disease resistance-related genes in Arabidopsis leaves were assessed. DAB and NBT staining showed deeper brown and purple colours in the leaves of treated plants than in those of the negative control plants (Fig. 4G). In addition, H_2DCFDA (DCF) fluorescence showed that NEO-, GSH-, and GSSG-induced ROS accumulation peaked at 4 hpt (Fig. 4H). Callose deposition is one of the most important cellular defence responses, and aniline blue staining was used to detect this phenomenon. There was a significant induction of callose deposition under the NEO, GSH, and GSSG treatments compared

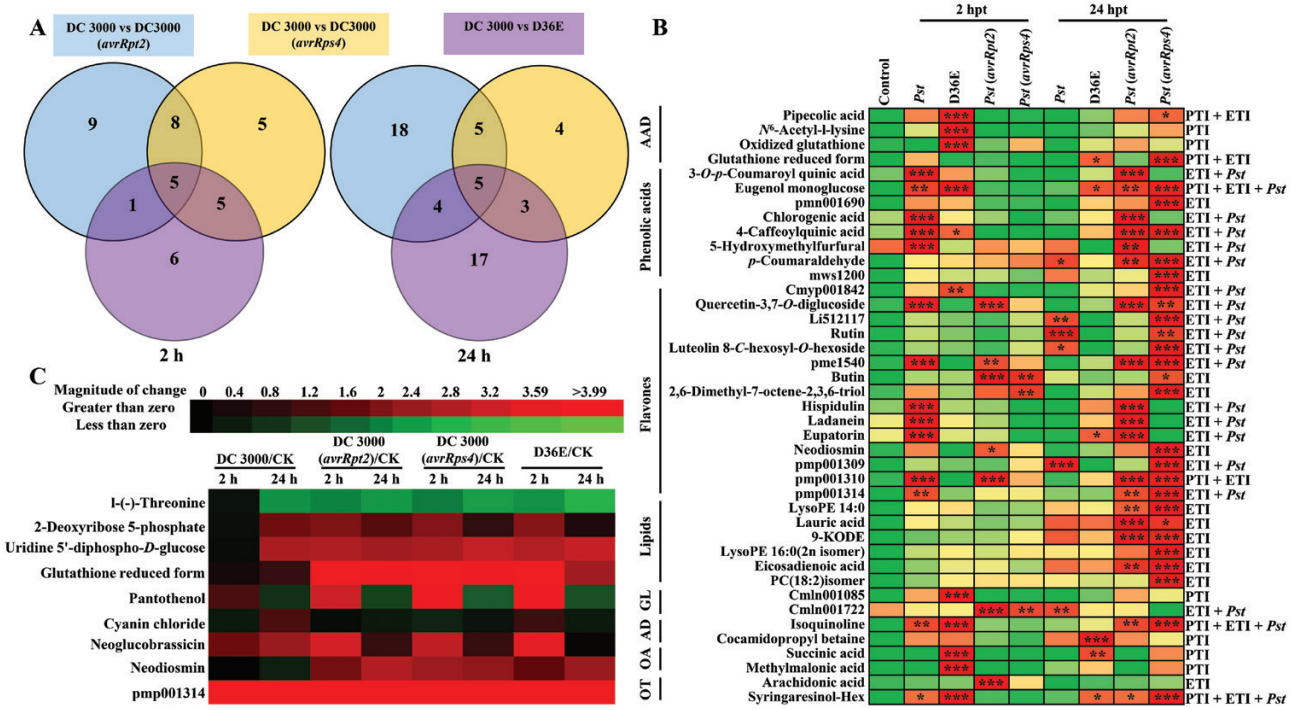

Fig. 3. Venn diagram combined with heatmap analysis showing that ETI and PTI jointly induced the accumulation of GSH and NEO at 2 hpt and 24 hpt. (A) Venn diagram representation of unique and shared differentially accumulated metabolites in DC 3000 vs. DC3000 (*avrRpt2*), DC 3000 vs. DC3000 (*avrRps4*), and DC 3000 vs. D36E at 2 hpt and 24 hpt. (B) Heatmap analysis showing GSH and NEO typically induced during ETI and PTI at 2 hpt and 24 hpt. OT: others, OA: organic acids, AD: alkaloids, GL: glucosinolates, AAD: amino acids and their derivatives. (C) Classification of metabolites co-regulated and specifically regulated by ETI and PTI. pmn001690, 3-hydroxy-4-isopropylbenzyl alcohol 3-glucoside; mws1200, trans-4-hydroxycinnamic acid methyl ester; Cmyp001842, kaempferol-malonyl-3-*O*-sophorotrioside; Li512117, quercetin 3-*O*-rhamnosyl-galactoside; pme1540, isorhamnetin 3-*O*-neohesperidoside; pmp001309, 6-hydroxykaempferol-7-*O*-glucoside; pmp001310, 6-hydroxykaempferol-3,6-*O*-diglucoside; pmp001314, 6-hydroxykaempferol-3-*O*-rutin-6-*O*-glucoside; Cmln001085, 2-hydroxy-2-methylbutyl thioglucoside (glucocleomin); Cmln001722, 6-(*p*-hydroxybenzoic acid)-β-D-1-thioglucoside of 4-(methylsulfinyl)-3-butenyl. The data are presented as the mean ±SE, n=3, **P*<0.05, ***P*<0.01, ****P*<0.001, based on Student's *t*-tests.

with the control treatment (Fig. 4I-J), which suggests that the NEO, GSH, and GSSG treatments induced callose deposition in the plant leaves.

PR1 is considered a marker of the SA pathway, which is essential for plant resistance to *Pst* DC3000 (Zhang and Li, 2019); thus, we conducted qRT-PCR to analyse the expression of marker genes of SA signalling, including *WRKY18*, *WRKY70*, and *PR1* (Huot *et al.*, 2017). As expected, we observed significant up-regulation of the expression of the abovementioned genes at 2 hpt and 24 hpt (Supplementary Fig. S4). Taken together, these results show that glutathione and NEO can activate the classical plant immune response.

PRRs/co-receptors are required for glutathione and NEO to induce plant immunity

Two PRR/co-receptor Arabidopsis mutants, *fls2 efr cerk1* (*fec*) and *bak1 bkk1 cerk1* (*bbc*), were found to be deficient in the recognition of almost all PAMPs due to a lack of major PRRs/co-receptors (Gimenez-Ibanez *et al.*, 2009; Schwessinger *et al.*, 2011; Macho and Zipfel, 2014; Xin *et al.*, 2016). As shown in Fig. 5A-C, NEO, GSH, or GSSG did not induce an effective immune response against *Pst* DC3000 in the *bbc* mutant or the *fec* mutant. RESPIRATORY BURST OXIDASE HOMOLOG D (RBOHD) plays a prominent role in pathogen-induced ROS production (Torres *et al.*, 2002; Kadota *et al.*, 2014; Li *et al.*, 2014). As shown in Fig. 5A, D, NEO, GSH, or GSSG failed to enhance plant resistance to pathogens in *rbohd* plants. According to the above results, GSSG-, GSH-, and NEO-induced plant disease resistance to pathogens relies on PRRs/co-receptors and *RBOHD*. AvrRpt2 was recognized by RESISTANCE TO *P. SYRINGAE 2* (RPS2) to activate the ETI response in wild-type Arabidopsis plants (Axtell and Staskawicz, 2003). As shown in Fig. 5E, GSH, GSSG, or NEO failed to significantly enhance plant resistance to *Pst* DC3000 in *rps2*.

To determine the effects of GSSG, GSH, and NEO on the regulation of the expression of ETI and PTI signalling pathway-related genes, further analysis of the PTI and ETI signalling marker genes at the transcriptome level was performed. We found that the expression of PTI signalling marker genes such as *RBOHD*, *MKK4*, *MPK3*, and *FRK1* (Asai *et al.*, 2002; Yuan *et al.*, 2021) was significantly higher in the Col-0 plants than in the *bbc*, *fec*, *rbohd*, and *rps2* mutants after GSSG, GSH,

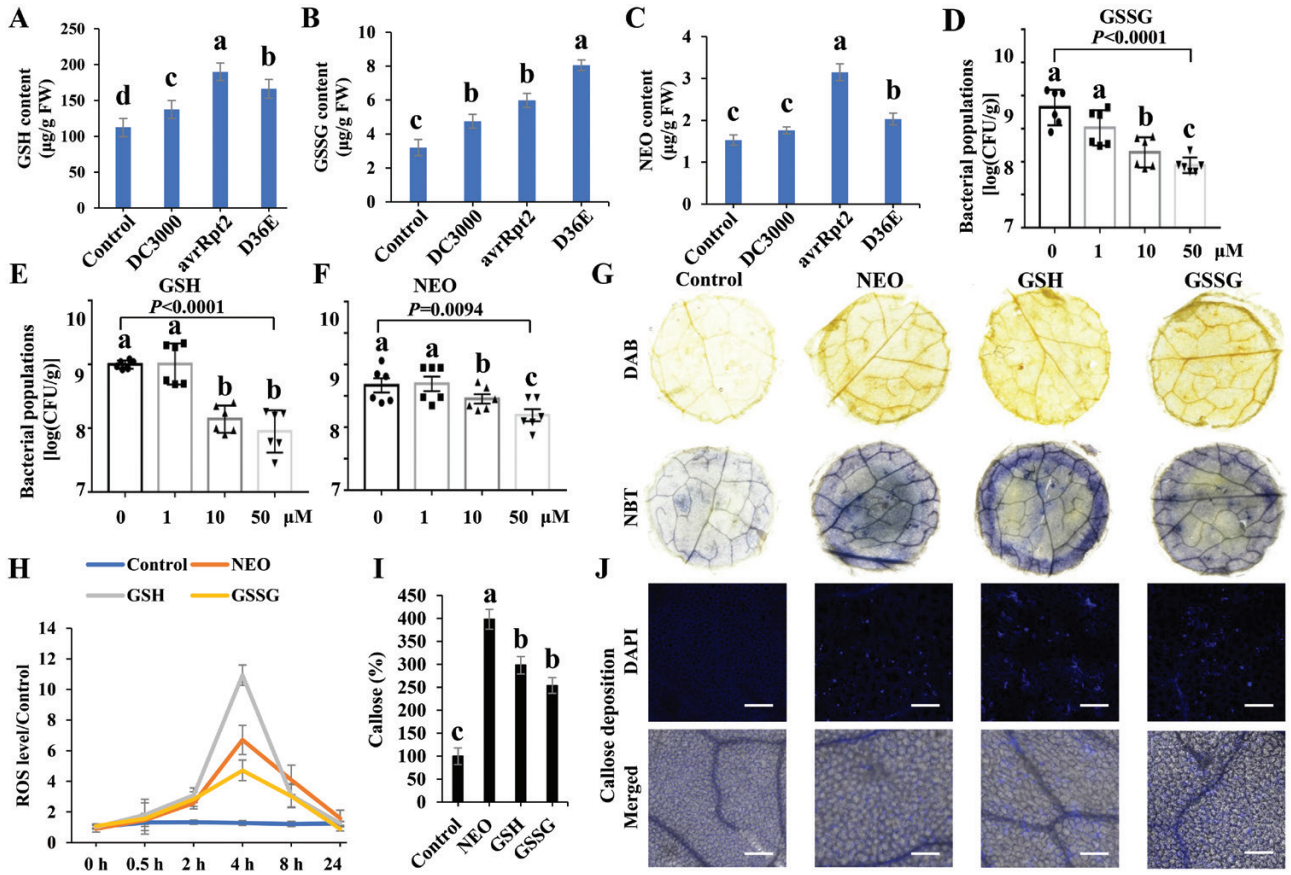

Fig. 4. GSH, GSSG, and NEO activate plant immunity. (A-C) Detection of GSH, GSSG, and NEO contents in Col-0 leaves, respectively. Plant leaves (mean ±SE, *n*=4, leaves from different independent plants) were pre-inoculated with DC3000 (OD_{600}=0.001), DC3000 (*avrRpt2*) (OD_{600}=0.001), and D36E (OD_{600}=0.001). Plant endogenous GSH, GSSG, and NEO contents were detected at 24 hpt by HPLC. Different letters represent significant differences between different groups (*P*<0.05 based on Student's *t*-test). (D-F) *Pst* DC3000 populations in Col-0 plant leaves (mean ±SE, *n*=4, leaves from different independent plants and repeated three times with similar results) after GSSG, GSH, and NEO treatment, respectively. Col-0 plant leaves were pre-sprayed with H_2O (control) or 1, 10, or 50 μM GSSG, GSH, or NEO and then inoculated with *Pst* DC3000 (OD_{600}=0.001) 2 h later. Bacterial populations were quantified at 3 dpi, log=log_{10}. Different letters represent significant differences between different groups (*P*<0.05 based on Student's *t*-test). (G) GSH-, GSSG-, and NEO-induced ROS accumulation. Col-0 plant leaves (*n*=6, leaves from different independent plants) were pre-sprayed with H_2O (control) or 50 μM GSH, GSSG, or NEO, and then H_2O_2 and O_2^- were detected by using DAB and NBT staining 2 h later, respectively. (H) The relative ROS content was detected at the indicated times. Col-0 plant leaves (mean ±SE, *n*=6, leaves from different independent plants) were pre-sprayed with H_2O (control) or 50 μM GSH, GSSG, or NEO and then the relative content of ROS was detected using the fluorescent dye H_2DCF-DA staining at 0, 0.5, 2, 4, 8, and 24 h later. (I) Callose content was quantified using ImageJ software. (J) GSH-, GSSG-, and NEO-induced callose deposition in Arabidopsis leaves. DAPI: callose fluorescence. Merged: overlay of callose fluorescence with bright field images. Col-0 plant leaves (mean ±SE, *n*=6, leaves from different independent plants) were pre-sprayed with H_2O (control) or 50 μM GSH, GSSG, or NEO and then callose was determined using aniline blue staining 24 h later. Different letters represent significant differences between different groups (*P*<0.05 based on Student's *t*-test).

and NEO treatment (Fig. 5F-K; Supplementary Fig. S5A-F), qPCR primers are listed in Supplementary Table S1. Additionally, the expression of ETI marker genes (*AZI1* and *EARLI1*) (Cecchini *et al.*, 2015) was significantly induced in Col-0 plants after GSSG, GSH, or NEO treatment compared with the control, but the fold changes in the expression of these genes were also reduced in the *bbc*, *fec*, *rbohd*, and *rps2* mutants (Fig. 5F-K; Supplementary Fig. S5A-F).

MPKs are important for plant defence against pathogen invasion (Meng and Zhang, 2013). Our results showed that GSSG, GSH, and NEO induced strong phosphorylation of MPKs in Col-0 plants, but failed to activate MPK phosphorylation in *bbc*, *fec*, and *rbohd* mutant plants (Fig. 5L). Together, these results indicate that both PRRs/co-receptors and *RBOHD* are required for GSSG-, GSH-, and NEO-mediated activation of ROS bursts and MPK phosphorylation. Interestingly, we observed normal GSSG- and GSH-induced phosphorylation of MPKs beyond NEO in *rps2* leaves. Together, these results indicate that PRRs/co-receptors and *RBOHD* are required for GSSG, GSH, and NEO activation of MPK phosphorylation, and that NEO-induced MPK phosphorylation also depends on *RPS2*.

ROS play an essential role in the activation of plant immunity. To investigate whether PRRs/co-receptors are required

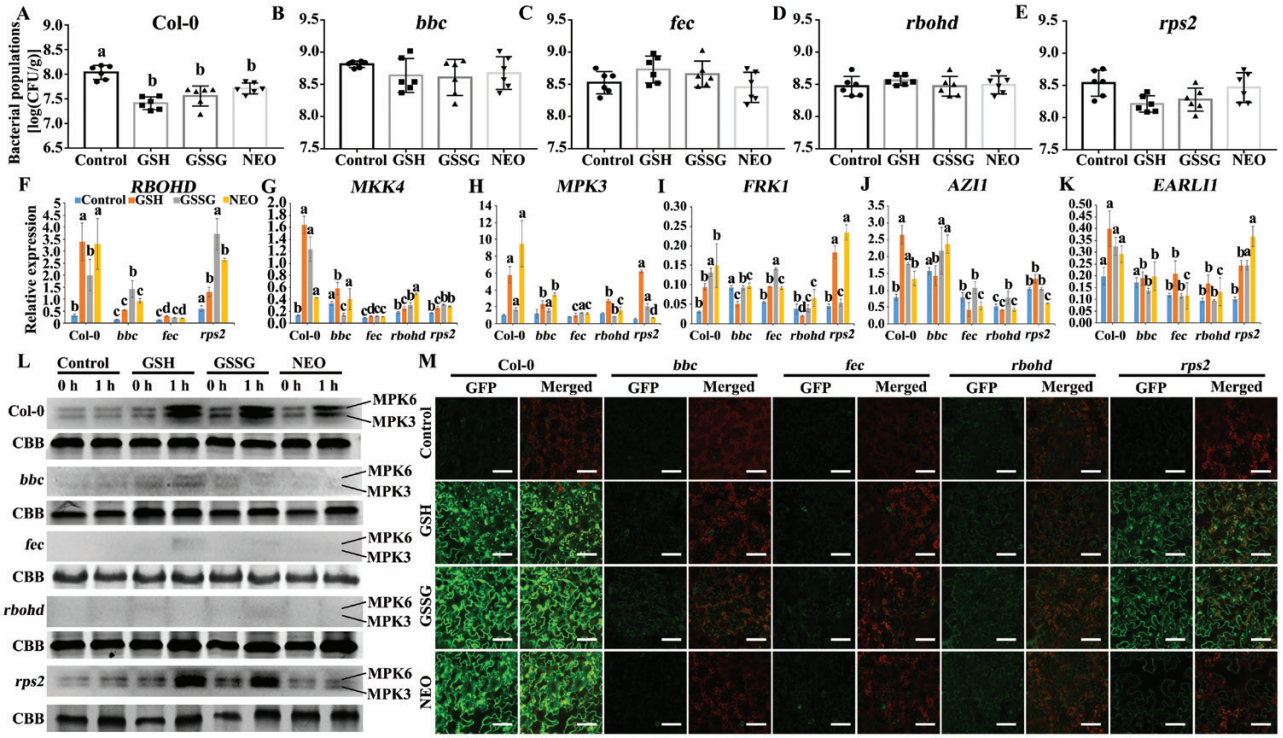

Fig. 5. GSH, GSSG, and NEO induce plant immunity depending on PRRs/co-receptors. (A-E) *Pst* DC3000 populations in Col-0, and *bbc*, *fec*, *rbohd*, and *rps2* mutant plant leaves, respectively. Plant leaves (mean ±SE, *n*=6, leaves from different independent plants with three biological repeats) were pre-sprayed with H_2O (control) or 50 μM GSH, GSSG, or NEO, and then inoculated with *Pst* DC3000 (OD_{600}=0.001) 2 h later. The bacterial population was measured at 2 dpi. log represents log_{10}. (F-K) qRT-PCR analysis of *RBOHD*, *MKK4*, *MPK3*, *FRK1*, *AZI1*, and *EARLI1* expression levels, respectively, in Col-0 and *bbc*, *fec*, *rbohd*, and *rps2* mutant plant leaves. Plant leaves (mean ±SE, *n*=4, leaves from different independent plants with three biological repeats) were pre-sprayed with H_2O (control) or 50 μM GSH, GSSG, or NEO, and then the treated leaves were harvested 2 h later, and total RNA was extracted for qPCR analysis. The *ACTIN* gene was used as an internal reference gene. Different letters represent significant differences between Col-0 and different groups (P<0.05 based on Student's *t*-test). (L) Phosphorylation of MPKs in Col-0 and *bbc*, *fec*, *rbohd*, and *rps2* plant leaves. CBB, Coomassie brilliant blue. Plant leaves (*n*=4, leaves from different independent plants) were pre-treated with H_2O (control) or 50 μM GSH, GSSG, or NEO, and MPK phosphorylation was detected at the indicated times. (M) ROS burst detection using fluorescent dye H_2DCFDA staining in Col-0, *bbc*, *fec*, *rbohd*, and *rps2* plant leaves. Plant leaves (*n*=4, leaves from different independent plants) were pre-sprayed with 50 μM GSH, GSSG, or NEO, and then the ROS burst was detected 2 h later. Bar=25 μm.

for ROS production induced by GSSG, GSH, and NEO, we evaluated ROS accumulation by applying the fluorescent dye H_2DCFDA to the leaves of Col-0, and the *bbc*, *fec*, *rbohd*, and *rps2* mutant plants. After GSSG, GSH, and NEO treatment, we observed a strong fluorescent signal in the leaves of Col-0 plants; however, the fluorescent signal was nearly undetectable in the leaves of *rbohd*, *bbc*, and *fec* plants (Fig. 5M), which demonstrated that GSSG-, GSH-, and NEO-induced ROS production depends on PRRs/co-receptors.

GSH1 *is involved in PTI and ETI*

To further determine the effect of plant endogenous glutathione on plant immunity, *gsh1*, a glutathione-reduced mutant plant (Cobbett *et al.*, 1998), was used for the following assays. Compared with Col-0, we found that *gsh1* was more susceptible to *Pst* DC3000 after water (control), *Pst* DC3000 (*avrRpt2*), and D36E pre-treatment for 2 h (Fig. 6A). Furthermore, we next examined the ROS burst, MPK phosphorylation and the expression of ETI and PTI signalling pathway-related genes in *gsh1*, and found that they were less strongly induced by *Pst* DC3000 (*avrRpt2*) and D36E inoculation in *gsh1* plants than in Col-0 plants (Fig. 6B-D). In addition, exogenous GSH and GSSG increased the content of plant endogenous GSH and GSSG in Col-0 and the *gsh1* mutant (Fig. 6E-F), and restored *gsh1* resistance to *Pst* DC3000 (Fig. 6G). Accordingly, the abovementioned results indicated that GSH and GSSG play an essential role in PTI and ETI.

Discussion

GSH, GSSG, and NEO are all described as important antioxidants, and a recent study reported that GSH plays an important role as an antioxidant for plants against viruses (Zhu *et al.*, 2021). However, previous studies have reported that flavonoid antioxidants, such as rutin and quercetin, can induce

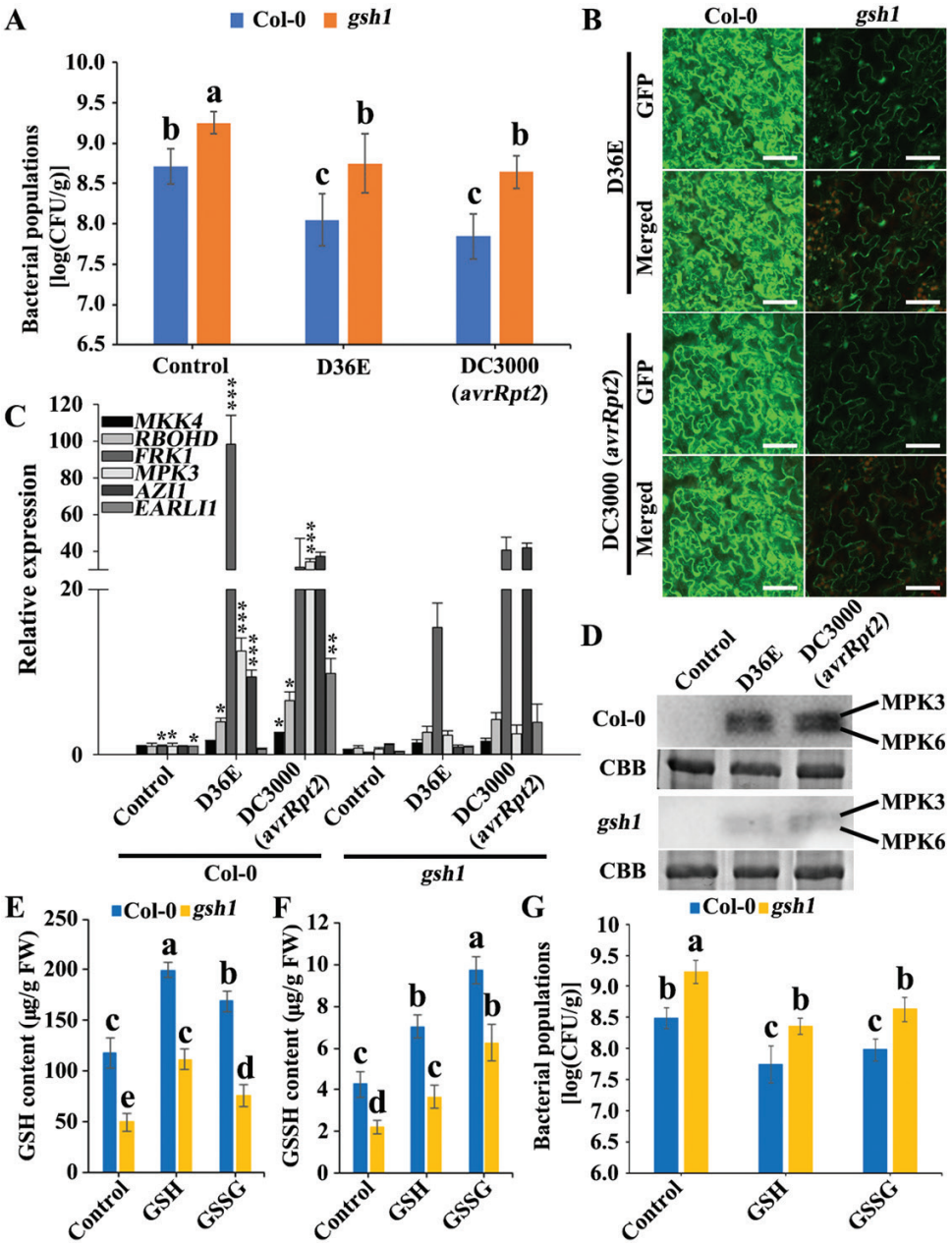

Fig. 6. *GSH1* is required for ETI and PTI. (A) *Pst* DC3000 bacterial populations in Col-0 and *gsh1* plant leaves. Plant leaves (mean ±SE, *n*=6, leaves from different independent plants with three biological repeats) were pre-treated with 10 mM $MgCl_2$ (control) or D36E (OD_{600}=0.02) or *Pst* DC3000 (*avrRpt2*) (OD_{600}=0.02) in 10 mM $MgCl_2$, and then inoculated with *Pst* DC3000 (OD_{600}=0.001) 2 h later. The bacterial population was measured at 2 dpi. D36E and *Pst* DC3000 (*avrRpt2*) were used to mimic PTI and ETI. log represents log_{10}. (B) ROS burst detection using fluorescent dye H_2DCFDA staining in Col-0 and *gsh1* plant leaves. Plant leaves (*n*=6, leaves from different independent plants) were pre-treated with 10 mM $MgCl_2$ (control) or D36E (OD_{600}=0.02) or *Pst* DC3000 (*avrRpt2*) (OD_{600}=0.02) in 10 mM $MgCl_2$, and then a ROS burst was detected 2 h later. D36E and *Pst* DC3000 (*avrRpt2*) were used to mimic PTI and ETI. Bar=50 μm. (C) qRT-PCR analysis of *RBOHD*, *MKK4*, *MPK3*, *FRK1*, *AZI1*, and *EARLI1* expression levels in Col-0 and *gsh1* plant leaves. Plant leaves (mean ±SE, *n*=6, leaves from different independent plants) were pre-treated with 10 mM $MgCl_2$ (control) or D36E (OD_{600}=0.02) or *Pst* DC3000 (*avrRpt2*) (OD_{600}=0.02) in 10 mM $MgCl_2$, and then the treated leaves were harvested 2 h later, and total RNA was extracted for qPCR analysis. Different letters represent significant differences between Col-0 and *gsh1* (P<0.05 based on Student's *t*-test). (D) Phosphorylation of MPKs in Col-0 and *gsh1* plant leaves. Plant leaves (*n*=4, leaves from different independent plants) were pre-treated with 10 mM $MgCl_2$ (control), or D36E (OD_{600}=0.02) or *Pst* DC3000 (*avrRpt2*) (OD_{600}=0.02) in 10 mM $MgCl_2$, and MPK phosphorylation was detected at the indicated times. (E-F) Detection of GSH, GSSG, and NEO contents in Col-0 and *gsh1* leaves. Plant leaves (mean ±SE, *n*=10, leaves from different independent plants) were pre-sprayed with 50 μM GSH, GSSG, or NEO, and plant endogenous GSH, GSSG, and NEO contents were detected at 24 hpt by HPLC. Different letters represent significant differences between different groups (P<0.05 based on Student's *t*-test). (G) *Pst* DC3000 bacterial populations in Col-0 and *gsh1* plant leaves. Plant leaves (mean ±SE, *n*=6, leaves from different independent plants with three biological repeats) were pre-treated with water (control) or 50 μM GSH, GSSG, or NEO, and then inoculated with *Pst* DC3000 (OD_{600}=0.001) 2 h later. The bacterial population was measured at 2 dpi. Different letters represent significant differences between different groups (P<0.05 based on Student's *t*-test).

plant immune responses, including up-regulating disease resistance gene expression and ROS bursts (Jia *et al.*, 2010; Yang *et al.*, 2016). Here, we found a novel role for the antioxidants GSH, GSSG, and NEO in plant immune responses. From these data, we propose the following model to summarize our findings (Fig. 7). Both PTI and ETI can trigger the accumulation of GSSG, GSH, and NEO in plant leaves. In turn, GSSG, GSH, and NEO induce ROS bursts, ETI- and PTI-associated gene expression and MPK phosphorylation to form a feedback loop to sustain the plant immune response. GSSG, GSH, and NEO induced the abovementioned immune responses in Col-0 plants but failed to do so in the *bbc* and *fec* mutants, which indicated that PRRs/co-receptors are the most important components for GSSG-, GSH-, and NEO-induced plant immunity. ROS bursts, MPK phosphorylation, and increased ETI- and PTI-associated gene expression were also compromised in the *rbohd* mutant, which indicates that ROS production is important for GSSG-, GSH-, and NEO-triggered plant immunity.

Exogenous glutathione may act as a damage-associated molecular pattern (DAMP) to activate plant immunity

GSH is a small peptide composed of glycine, cysteine, and glutamate. GSH is also an important antioxidant and plays an important role in the defence against abiotic stress in plants (Dubreuil-Maurizi and Poinssot, 2012; Nianiou-Obeidat *et al.*, 2017). In addition, recent research has shown that GSH can enhance plant resistance to tobacco mosaic virus by reducing the damage of excessive ROS to plant cells (Zhu *et al.*, 2021), or conjugate with toxic epoxide moieties to detoxify deoxynivalenol and confer plant resistance to *Fusarium* head blight (Wang *et al.*, 2020). Similarly, we also found that GSH is induced by PTI, and discovered a novel function of GSH in regulating plant immunity. In our study, we found that GSH also directly induced a ROS burst, MPK phosphorylation, and plant resistance to pathogens (Fig. 5). In addition, GSH-induced plant immunity is compromised in the PRR/co-receptor-deficient

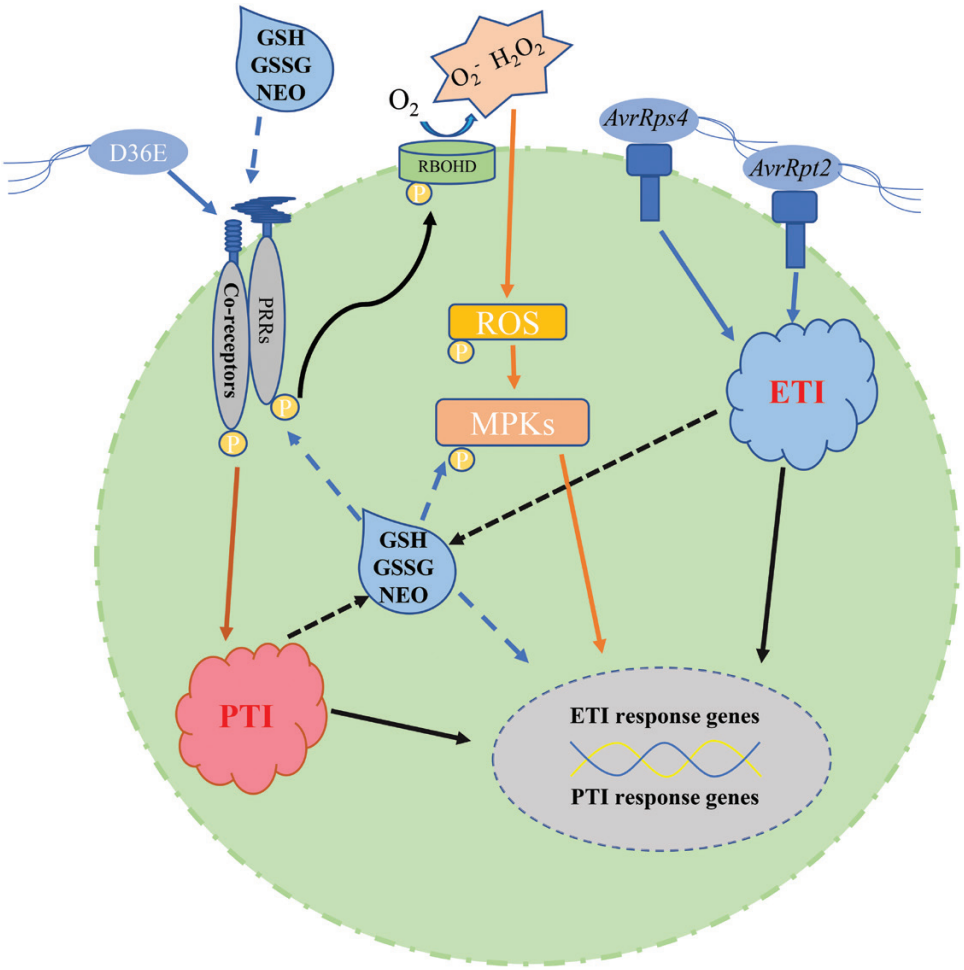

Fig. 7. Model of glutathione and NEO in triggering plant immunity. The model describes the findings of this study, showing that glutathione and NEO are the key metabolites involved in the response to ETI and PTI. The accumulation of GSH, GSSG, and NEO is induced by ETI or PTI, which further activates the ROS burst, MPK phosphorylation, and ETI- and PTI-associated gene reprogramming depending on PRRs/co-receptors.

plants *bbc* and *fec*, which indicates that GSH-induced plant resistance requires PRRs/co-receptors. These results suggest that GSH fits the characteristics of DAMPs. Based on this evidence, we propose that GSH may act as a DAMP to activate plant immunity.

GSH1 *plays a role in plant immunity*

GSH biosynthesis genes are also involved in plant-pathogen interactions. Decades ago, a glutathione-deficient mutant (*gsh1*) was reported to be more sensitive to pathogens (Mike *et al.*, 1995). However, how *GSH1* regulates plant immune responses remains unclear. In this study, we found that D36E and *Pst* DC3000 (*avrRpt2*) failed to enhance *gsh1* resistance to *Pst* DC3000 compared with Col-0. Furthermore, we also found that D36E and *Pst* DC3000 (*avrRpt2*) are unable to induce a ROS burst and MPK phosphorylation effectively, which indicated that *GSH1* is involved in regulating ETI and PTI responses induced by D36E and *Pst* DC3000 (*avrRpt2*).

Neodiosmin and glutathione play a key role in triggering plant immunity

Plants accumulate large amounts of pathogen-related metabolites in response to pathogen invasion. In recent decades, a number of metabolites, such as salicylic acid, methyl-salicylic acid, azelaic acid, glycerol-3-phosphate, pipecolic acid, and the abietane diterpenoid, dehydroabietinal (Navarova *et al.*, 2012; Fu and Dong, 2013), have been reported to be involved in plant system-acquired immunity. However, we know very little about the immune compounds in response to plant-based ETI and PTI. Currently, our research fills the gap in this area. In our study, metabolomics data analysis showed that ETI and PTI induced the accumulation of large amounts of flavonoids, and amino acids and their derivatives, in inoculated plant leaves (Fig. 2; Supplementary Fig. S2). In the *Pst* DC3000 (*avrRpt2*)/CK, *Pst* DC3000 (*avrRps4*)/CK, and D36E/CK combinations, the contents of GSSG, GSH, and NEO at 2 hpt or 24 hpt significantly increased compared with those in the *Pst* DC3000/CK combination (Fig. 3). In contrast, the highly pathogenic strain *Pst* DC3000 inhibited the accumulation of NEO and glutathione, which indicated that NEO and glutathione play a role in ETI and PTI. A previous study reported that 1 mM GSH can scavenge excessive ROS accumulation to reduce cell damage in plant-virus interactions (Zhu *et al.*, 2021). However, the GSH concentration used in our study was 50 μM, which is much lower than 1 mM. Therefore, low concentrations (50 μM) of GSH, GSSG, and NEO are more like an elicitor to activate plant immunity rather than a scavenger of excessive ROS, and previous studies have also shown that the antioxidants rutin and quercetin could activate plant immunity (Jia *et al.*, 2010; Yang *et al.*, 2016). In addition, NEO- and glutathione-induced plant immune responses require PRRs/co-receptors (Fig. 5); accordingly, we speculate that GSH, NEO, and GSSG may also be recognized by receptors and transmit immune signals through PRRs/co-receptors. This study showed that the glutathione-reduced mutant plant *gsh1* showed a weaker immune response, including ROS bursts and MPK cascades and increased ETI- and PTI-associated gene expression, induced by *Pst* DC3000 (*avrRpt2*) and D36E, which suggested that glutathione is probably a plant immune response-associated metabolite. In summary, we propose that NEO and glutathione may be marker metabolites involved in plant immune responses.

The feedback function of NEO and glutathione in response to ETI and PTI

Together ETI and PTI are the most notable two-layered plant immune system for restricting pathogen invasion. Metabolic signals work cooperatively to protect plants from microbial pathogen invasion, especially in the process of activating systemic acquired resistance (SAR), which offers protection against a broad spectrum of pathogenic and non-pathogenic pathogens (Gao *et al.*, 2014). SAR can be primed by various signalling molecules, including methyl salicylate (MeSA), free radicals (nitric oxide and ROS), dicarboxylic acid azelaic acid (AzA), glycerol-3-phosphate (G3P), dehydroabietinal (DA), monoterpenes (α-pinene and β-pinene), NAD(P), lipid-transfer protein DIR1, the amino acid derivative pipecolic acid (Pip), and *N*-hydroxy-pipecolic acid (NHP) (Dempsey and Klessig, 2012; Hartmann *et al.*, 2018), which suggests that endogenous plant metabolites are very important for the regulation of plant immunity. Previous reports have shown that the flavonols NEO, rutin, hispidulin, ladanein, eupatorine, and prunetin are essential in the process of animal and plant antibacterial, anticancer, anti-insect, antiviral and antioxidative stress responses (Calland *et al.*, 2012; Yang *et al.*, 2016; Abd Razak *et al.*, 2020; Liu *et al.*, 2020; Raithore *et al.*, 2020; Vetrivel *et al.*, 2020; Ding *et al.*, 2021). NEO is also a flavone glycoside purified from plant leaves and functions as a strong antioxidant with potential value applications in beverage, food, and pharmaceutical storage (Raithore *et al.*, 2020). Here, we also found that the abovementioned metabolites were induced by ETI or PTI. Furthermore, we found that the contents of GSH and NEO accumulated significantly in response to *Pst* DC3000 (*avrRpt2*), *Pst* DC3000 (*avrRps4*), and D36E but not to the control or *Pst* DC3000, which indicated that GSH and NEO may participate in PTI and ETI responses. Moreover, we also determined the function of the glutathione oxidized form (GSSG) in triggering plant immunity. In terms of exploring the role of GSH, GSSG, and NEO in the regulation of plant immunity, our research showed that GSSG, GSH, and NEO significantly enhance plant resistance to pathogens and induce ROS bursts, MPK phosphorylation, and increased expression of ETI and PTI signalling pathway-related genes (Figs 4–6). To our knowledge, that GSSG, GSH, and NEO play an important role in ETI- and PTI-associated immune signal feedback is a novel discovery. Our results reveal that the plant immune

system utilizes amino acid derivatives (GSSG and GSH) and flavonoids (NEO) for feedback maintenance of plant immunity in plants, which is of great value for exploring the role of endogenous immune response-associated metabolites in plant immunity. These results might have potential practical implications, and as a strategy, plant immunity could be broadly increased to respond to pathogen invasion through the precise control of the content of GSSG, GSH, or NEO.

Supplementary data

The following supplementary data are available at *JXB* online.

Table S1. Sequences of primers used for qRT-PCR.

Fig. S1. Overall qualitative analysis of the metabolomics data.

Fig. S2. Amino acid metabolism after four *Pst* strain inoculations at 2 hpt and 24 hpt.

Fig. S3. Effects of NEO, GSSG, and GSH on the growth of *Pst* DC3000.

Fig. S4. qRT-PCR analysis of *WRKY18*, *WRKY70*, and *PR1* expression levels in Col-0 plants at 2 hpt and 24 hpt.

Fig. S5. (A-F) qRT-PCR analysis of *RBOHD*, *MKK4*, *MPK3*, *FRK1*, *AZI1*, and *EARLI1* expression levels in Col-0 and *bbc*, *fec*, *rbohd*, and *rps2* mutant plant leaves.

Acknowledgements

We thank Prof. Cyril Zipfel and Prof. Xiufang Xin for providing *bbc*, *fec*, *rbohd*, and *rps2* mutant seeds.

Author contributions

XD and CL conceived the project. CL performed experiments. XD and CL wrote the manuscript. YJ, YY, YS, MH, XK, QW, DC, and LW analysed the experimental data. BL, ZY, YL, HD, XL, XX, and YL analysed and provided valuable suggestions for this manuscript. All authors approved the final text.

Conflict of interest

QW and DC are employed by Shandong Pengbo Biotechnology Co., Ltd, Taian, Shandong, China. The remaining authors declare that the research was conducted in the absence of any commercial or financial relationships that could be construed as a potential conflict of interest.

Funding

The work was supported by the National Natural Science Foundation (32072500, 31872925, 32272557), Shandong Province Key Research and Development Plan (2020CXGC010803, 2021TZXD007-04-4), Science and Technology Support Plan for Youth Innovation of Colleges and Universities of Shandong Province (2019KJF023), Taishan Scholar Program of Shandong Province, Shandong Province Postdoctoral Innovation Project (202103027) and Natural Science Foundation of Shandong Province (ZR2022QC114, ZR2022ZD23).

Data availability

All data supporting the findings of this study are available within the article and within its supplementary materials published online. Raw metabolomics data and peak annotation parameters are available online in the Dryad Digital repository: https://doi.org/10.5061/dryad.dr7sqvb1w (Lu *et al.*, 2022).

References

Abd Razak N, Yeap SK, Alitheen NB, Ho WY, Yong CY, Tan SW, Tan WS, Long K. 2020. Eupatorin suppressed tumor progression and enhanced immunity in a 4T1 murine breast cancer model. Integrative Cancer Therapies **19**, 1534735420935625.

Ansorge WJ. 2009. Next-generation DNA sequencing techniques. New Biotechnology **25**, 195–203.

Asai T, Tena G, Plotnikova J, Willmann MR, Chiu WL, Gomez-Gomez L, Boller T, Ausubel FM, Sheen J. 2002. MAP kinase signalling cascade in Arabidopsis innate immunity. Nature **415**, 977–983.

Axtell MJ, Staskawicz BJ. 2003. Initiation of RPS2-specified disease resistance in Arabidopsis is coupled to the AvrRpt2-directed elimination of RIN4. Cell **112**, 369–377.

Calland N, Dubuisson J, Rouille Y, Seron K. 2012. Hepatitis C virus and natural compounds: a new antiviral approach? Viruses **4**, 2197–2217.

Cecchini NM, Steffes K, Schlappi MR, Gifford AN, Greenberg JT. 2015. Arabidopsis AZI1 family proteins mediate signal mobilization for systemic defence priming. Nature Communications **6**, 7658.

Chang M, Chen H, Liu F, Fu ZQ. 2021. PTI and ETI: convergent pathways with diverse elicitors. Trends in Plant Science **27**, 113–115.

Chaouch S, Queval G, Noctor G. 2012. AtRbohF is a crucial modulator of defence-associated metabolism and a key actor in the interplay between intracellular oxidative stress and pathogenesis responses in Arabidopsis. The Plant Journal **69**, 613–627.

Chen W, Gong L, Guo Z, Wang W, Zhang H, Liu X, Yu S, Xiong L, Luo J. 2013. A novel integrated method for large-scale detection, identification, and quantification of widely targeted metabolites: application in the study of rice metabolomics. Molecular Plant **6**, 1769–1780.

Cheng MC, Ko K, Chang WL, Kuo WC, Chen GH, Lin TP. 2015. Increased glutathione contributes to stress tolerance and global translational changes in Arabidopsis. The Plant Journal **83**, 926–939.

Clay NK, Adio AM, Denoux C, Jander G, Ausubel FM. 2009. Glucosinolate metabolites required for an Arabidopsis innate immune response. Science **323**, 95–101.

Cobbett CS, May MJ, Howden R, Rolls B. 1998. The glutathione-deficient, cadmium-sensitive mutant, cad2-1, of *Arabidopsis thaliana* is deficient in gamma-glutamylcysteine synthetase. The Plant Journal **16**, 73–78.

Couto D, Zipfel C. 2016. Regulation of pattern recognition receptor signalling in plants. Nature Reviews Immunology **16**, 537–552.

Cunnac S, Chakravarthy S, Kvitko BH, Russell AB, Martin GB, Collmer A. 2011. Genetic disassembly and combinatorial reassembly identify a minimal functional repertoire of type III effectors in *Pseudomonas syringae*. Proceedings of the National Academy of Sciences, USA **108**, 2975–2980.

Dempsey DA, Klessig DF. 2012. SOS - too many signals for systemic acquired resistance? Trends in Plant Science **17**, 538–545.

De Vleesschauwer D, Seifi HS, Filipe O, Haeck A, Huu SN, Demeestere K, Hofte M. 2016. The DELLA protein SLR1 integrates and

amplifies salicylic acid- and jasmonic acid-dependent innate immunity in rice. Plant Physiology **170**, 1831–1847.

Ding X, Zhang H, Li M, Yin Z, Chu Z, Zhao X, Li Y, Ding X. 2021. AtMYB12-expressing transgenic tobacco increases resistance to several phytopathogens and aphids. Frontiers in Agronomy **3, doi: 10.3389/fagro.2021.694333**.

Dodds PN, Rathjen JP. 2010. Plant immunity: towards an integrated view of plant-pathogen interactions. Nature Reviews Genetics **11**, 539–548.

Dubreuil-Maurizi C, Poinssot B. 2012. Role of glutathione in plant signaling under biotic stress. Plant Signaling & Behavior **7**, 210–212.

Fu ZQ, Dong X. 2013. Systemic acquired resistance: turning local infection into global defense. Annual Review of Plant Biology **64**, 839–863.

Gao QM, Kachroo A, Kachroo P. 2014. Chemical inducers of systemic immunity in plants. Journal of Experimental Botany **65**, 1849–1855.

Gassmann W, Hinsch ME, Staskawicz BJ. 1999. The Arabidopsis RPS4 bacterial-resistance gene is a member of the TIR-NBS-LRR family of disease-resistance genes. The Plant Journal **20**, 265–277.

Gimenez-Ibanez S, Ntoukakis V, Rathjen JP. 2009. The LysM receptor kinase CERK1 mediates bacterial perception in Arabidopsis. Plant Signaling & Behavior **4**, 539–541.

Griebel T, Zeier J. 2010. A role for beta-sitosterol to stigmasterol conversion in plant-pathogen interactions. The Plant Journal **63**, 254–268.

Haas BJ, Zody MC. 2010. Advancing RNA-Seq analysis. Nature Biotechnology **28**, 421–423.

Hartmann M, Zeier T, Bernsdorff F, Reichel-Deland V, Kim D, Hohmann M, Scholten N, Schuck S, Brautigam A, Holzel T, Ganter C, Zeier J. 2018. Flavin monooxygenase-generated N-hydroxypipecolic acid is a critical element of plant systemic immunity. Cell **173**, 456–469.e16.

Huang J, Lu YJ, Guo C, Zuo S, Zhou JL, Wong WL, Huang B. 2021. The study of citrus-derived flavonoids as effective bitter taste inhibitors. Journal of the Science of Food and Agriculture **101**, 5163–5171.

Huot B, Castroverde CDM, Velasquez AC, Hubbard E, Pulman JA, Yao J, Childs KL, Tsuda K, Montgomery BL, He SY. 2017. Dual impact of elevated temperature on plant defence and bacterial virulence in Arabidopsis. Nature Communications **8**, 1808.

Jia Z, Zou B, Wang X, Qiu J, Ma H, Gou Z, Song S, Dong H. 2010. Quercetin-induced H_2O_2 mediates the pathogen resistance against *Pseudomonas syringae* pv. *tomato* DC3000 in *Arabidopsis thaliana*. Biochemical and Biophysical Research Communications **396**, 522–527.

Jones JD, Dangl JL. 2006. The plant immune system. Nature **444**, 323–329.

Jones JD, Vance RE, Dangl JL. 2016. Intracellular innate immune surveillance devices in plants and animals. Science **354, doi: 10.1126/science.aaf63**.

Kadota Y, Sklenar J, Derbyshire P, *et al*. 2014. Direct regulation of the NADPH oxidase RBOHD by the PRR-associated kinase BIK1 during plant immunity. Molecular Cell **54**, 43–55.

Kocsy G, von Ballmoos P, Suter M, Ruegsegger A, Galli U, Szalai G, Galiba G, Brunold C. 2000. Inhibition of glutathione synthesis reduces chilling tolerance in maize. Planta **211**, 528–536.

Kunstler A, Kiraly L, Katay G, Enyedi AJ, Gullner G. 2019. Glutathione can compensate for salicylic acid deficiency in tobacco to maintain resistance to tobacco mosaic virus. Frontiers in Plant Science **10**, 1115.

Li S, Dong X, Fan G, *et al*. 2018. Comprehensive profiling and inheritance patterns of metabolites in foxtail millet. Frontiers in Plant Science **9**, 1716.

Li L, Li M, Yu L, *et al*. 2014. The FLS2-associated kinase BIK1 directly phosphorylates the NADPH oxidase RbohD to control plant immunity. Cell Host & Microbe **15**, 329–338.

Liu L, Sonbol FM, Huot B, Gu Y, Withers J, Mwimba M, Yao J, He SY, Dong X. 2016. Salicylic acid receptors activate jasmonic acid signalling through a non-canonical pathway to promote effector-triggered immunity. Nature Communications **7**, 13099.

Liu H, Zhang B, Wu T, Ding Y, Ding X, Chu Z. 2015. Copper ion elicits defense response in *Arabidopsis thaliana* by activating salicylate- and ethylene-dependent signaling pathways. Molecular Plant **8**, 1550–1553.

Liu K, Zhao F, Yan J, Xia Z, Jiang D, Ma P. 2020. Hispidulin: a promising flavonoid with diverse anti-cancer properties. Life Sciences **259**, 118395.

Lu CC, Liu HF, Jiang DP, *et al*. 2019. *Paecilomyces variotii* extracts (ZNC) enhance plant immunity and promote plant growth. Plant and Soil **441**, 383–397.

Lu C, Jiang Y, Yue Y, *et al*. 2022. Data from: Glutathione and neodiosmin feedback sustain plant immunity. [Dataset] Dryad Digital Repository. https://doi.org/10.5061/dryad.dr7sqvb1w

Macho AP, Zipfel C. 2014. Plant PRRs and the activation of innate immune signaling. Molecular Cell **54**, 263–272.

Mackey D, Belkhadir Y, Alonso JM, Ecker JR, Dangl JL. 2003. Arabidopsis RIN4 is a target of the type III virulence effector AvrRpt2 and modulates RPS2-mediated resistance. Cell **112**, 379–389.

Meng X, Zhang S. 2013. MAPK cascades in plant disease resistance signaling. Annual Review of Phytopathology **51**, 245–266.

Mike J, May JEP, Daniels MJ, Leaver CJ, Cobbett CS. 1995. An Arabidopsis mutant depleted in glutathione shows unaltered responses to fungal and bacterial pathogens. Molecular Plant-Microbe Interactions **9**, 349–356.

Monaghan J, Zipfel C. 2012. Plant pattern recognition receptor complexes at the plasma membrane. Current Opinion in Plant Biology **15**, 349–357.

Mukaihara T, Hatanaka T, Nakano M, Oda K. 2016. *Ralstonia solanacearum* Type III effector RipAY is a glutathione-degrading enzyme that is activated by plant cytosolic thioredoxins and suppresses plant immunity. mBio **7**, e00359–e00316.

Mur LA, Brown IR, Darby RM, Bestwick CS, Bi YM, Mansfield JW, Draper J. 2000. A loss of resistance to avirulent bacterial pathogens in tobacco is associated with the attenuation of a salicylic acid-potentiated oxidative burst. The Plant Journal **23**, 609–621.

Navarova H, Bernsdorff F, Doring AC, Zeier J. 2012. Pipecolic acid, an endogenous mediator of defense amplification and priming, is a critical regulator of inducible plant immunity. The Plant Cell **24**, 5123–5141.

Ngou BPM, Ahn HK, Ding P, Jones JDG. 2021. Mutual potentiation of plant immunity by cell-surface and intracellular receptors. Nature **592**, 110–115.

Nianiou-Obeidat I, Madesis P, Kissoudis C, Voulgari G, Chronopoulou E, Tsaftaris A, Labrou NE. 2017. Plant glutathione transferase-mediated stress tolerance: functions and biotechnological applications. Plant Cell Reports **36**, 791–805.

Nobori T, Velasquez AC, Wu J, Kvitko BH, Kremer JM, Wang Y, He SY, Tsuda K. 2018. Transcriptome landscape of a bacterial pathogen under plant immunity. Proceedings of the National Academy of Sciences, USA **115**, E3055–E3064.

Noctor G, Mhamdi A, Chaouch S, Han Y, Neukermans J, Marquez-Garcia B, Queval G, Foyer CH. 2012. Glutathione in plants: an integrated overview. Plant Cell and Environment **35**, 454–484.

Oh CS, Martin GB. 2011. Effector-triggered immunity mediated by the Pto kinase. Trends in Plant Science **16**, 132–140.

Pedley KF, Martin GB. 2003. Molecular basis of Pto-mediated resistance to bacterial speck disease in tomato. Annual Review of Phytopathology **41**, 215–243.

Pombo MA, Zheng Y, Fernandez-Pozo N, Dunham DM, Fei Z, Martin GB. 2014. Transcriptomic analysis reveals tomato genes whose expression is induced specifically during effector-triggered immunity and identifies the Epk1 protein kinase which is required for the host response to three bacterial effector proteins. Genome Biology **15**, 492.

Raithore S, Kiefl J, Manthey JA, Plotto A, Bai J, Zhao W, Baldwin E. 2020. Mitigation of off-flavor in huanglongbing-affected orange juice using natural citrus non-volatile compounds. Journal of Agricultural and Food Chemistry **68**, 1038–1050.

Rosli HG, Zheng Y, Pombo MA, Zhong S, Bombarely A, Fei Z, Collmer A, Martin GB. 2013. Transcriptomics-based screen for genes induced by flagellin and repressed by pathogen effectors identifies a cell wall-associated kinase involved in plant immunity. Genome Biology **14**, R139.

Schwessinger B, Roux M, Kadota Y, Ntoukakis V, Sklenar J, Jones A, Zipfel C. 2011. Phosphorylation-dependent differential regulation of plant

growth, cell death, and innate immunity by the regulatory receptor-like kinase BAK1. PLoS Genetics **7**, e1002046.

Segonzac C, Zipfel C. 2011. Activation of plant pattern-recognition receptors by bacteria. Current Opinion in Microbiology **14**, 54–61.

Stahl E, Bellwon P, Huber S, Schlaeppi K, Bernsdorff F, Vallat-Michel A, Mauch F, Zeier J. 2016. Regulatory and functional aspects of indolic metabolism in plant systemic acquired resistance. Molecular Plant **9**, 662–681.

Tang B, Liu C, Li Z, Zhang X, Zhou S, Wang GL, Chen XL, Liu W. 2021. Multilayer regulatory landscape during pattern-triggered immunity in rice. Plant Biotechnology Journal **19**, 2629–2645.

Torres MA, Dangl JL, Jones JD. 2002. Arabidopsis gp91phox homologues AtrbohD and AtrbohF are required for accumulation of reactive oxygen intermediates in the plant defense response. Proceedings of the National Academy of Sciences, USA **99**, 517–522.

Tsuda K, Katagiri F. 2010. Comparing signaling mechanisms engaged in pattern-triggered and effector-triggered immunity. Current Opinion in Plant Biology **13**, 459–465.

Vetrivel P, Kim SM, Ha SE, Kim HH, Bhosale PB, Senthil K, Kim GS. 2020. Compound prunetin induces cell death in gastric cancer cell with potent anti-proliferative properties: in vitro assay, molecular docking, dynamics, and ADMET studies. Biomolecules **10**, 1086.

Wang Z, Gerstein M, Snyder M. 2009. RNA-Seq: a revolutionary tool for transcriptomics. Nature Reviews Genetics **10**, 57–63.

Wang H, Sun S, Ge W, *et al*. 2020. Horizontal gene transfer of Fhb7 from fungus underlies *Fusarium* head blight resistance in wheat. Science **368**, eaba5435.

Wei HL, Chakravarthy S, Mathieu J, Helmann TC, Stodghill P, Swingle B, Martin GB, Collmer A. 2015. *Pseudomonas syringae* pv. *tomato* DC3000 type III secretion effector polymutants reveal an interplay between HopAD1 and AvrPtoB. Cell Host & Microbe **17**, 752–762.

Xin XF, Nomura K, Aung K, Velasquez AC, Yao J, Boutrot F, Chang JH, Zipfel C, He SY. 2016. Bacteria establish an aqueous living space in plants crucial for virulence. Nature **539**, 524–529.

Yang W, Xu X, Li Y, Wang Y, Li M, Wang Y, Ding X, Chu Z. 2016. Rutin-mediated priming of plant resistance to three bacterial pathogens initiating the early SA signal pathway. PLoS One **11**, e0146910.

Yuan M, Jiang Z, Bi G, Nomura K, Liu M, Wang Y, Cai B, Zhou JM, He SY, Xin XF. 2021. Pattern-recognition receptors are required for NLR-mediated plant immunity. Nature **592**, 105–109.

Zechmann B. 2014. Compartment-specific importance of glutathione during abiotic and biotic stress. Frontiers in Plant Science **5**, 566.

Zhang Y, Li X. 2019. Salicylic acid: biosynthesis, perception, and contributions to plant immunity. Current Opinion in Plant Biology **50**, 29–36.

Zhu F, Zhang QP, Che YP, Zhu PX, Zhang QQ, Ji ZL. 2021. Glutathione contributes to resistance responses to TMV through a differential modulation of salicylic acid and reactive oxygen species. Molecular Plant Pathology **22**, 1668–1687.